

Intracluster Atomic and Electronic Structural Heterogeneities in Supported Nanoscale Metal Catalysts

Annika Elsen,^{†,∇} Ulrich Jung,^{†,∇} Fernando Vila,^{‡,∇} Yuanyuan Li,[§] Olga V. Safonova,^{||} Rowena Thomas,[⊥] Moniek Tromp,[#] John J. Rehr,^{*,‡} Ralph G. Nuzzo,^{*,†} and Anatoly I. Frenkel^{*,§}

[†]Department of Chemistry, University of Illinois, Urbana, Illinois 61801, United States

[‡]Department of Physics, University of Washington, Seattle, Washington 98195, United States

[§]Department of Physics, Yeshiva University, New York, New York 10033, United States

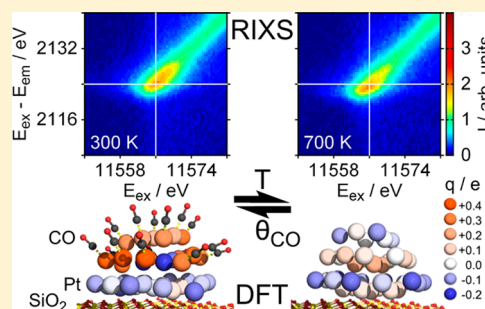
^{||}Paul Scherrer Institut, 5232 Villigen, Switzerland

[⊥]Catalysis Characterization, Catalysis Research Center, Technische Universität München, 803333 Munich, Germany

[#]Van 't Hoff Institute for Molecular Sciences, University of Amsterdam, 1012 Amsterdam, The Netherlands

S Supporting Information

ABSTRACT: This work reveals and quantifies the inherent intracluster heterogeneity in the atomic structure and charge distribution present in supported metal catalysts. The results demonstrate that these distributions are pronounced and strongly coupled to both structural and dynamic perturbations. They also serve to clarify the nature of the dynamic bonding of nanoscale catalytic metal clusters with their supports, and the mediation of these properties due to the presence of adsorbates. These findings are supported by theoretical modeling and experimental data measured for an exemplary supported metal catalyst, Pt supported on silica, using *in situ* high energy resolution X-ray absorption and emission spectroscopies; *in situ* diffuse reflectance infrared Fourier transform spectroscopy; and *ex situ* scanning transmission electron microscopy.



1. INTRODUCTION

There now exists abundant experimental and theoretical information that illustrates how the atomic structure and electronic properties of supported nanoscale metal cluster catalysts differ from those present in bulk solids. These effects include as notable examples the perturbations arising due to surface strains^{1,2} and changes in thermal, structural, magnetic, or optical properties due to cluster size effects.^{3–6} These findings lead to a view of a typical supported metal nanoparticle whose structure possesses a certain degree of heterogeneity, in which atoms on the surface of the cluster are relaxed and further subject to perturbations due to adsorbate bonding, while those in the interior maintain approximate order.^{4,7,8} In particular, the adsorption of H₂ and CO on Pt nanoparticle catalysts has been intensively studied by XAFS.^{9–16} Additional perturbations originating in the metal–support bonding interactions are also known to contribute to the structural, electronic, and catalytic properties of these systems.¹⁷ In this article, we report on heterogeneities observed in the intracluster distributions of both atoms and charges in supported metal clusters that are far more complex than those described above, and we raise a set of important questions: *What is the nature of these heterogeneities and what are their consequences for the physicochemical properties of nanoscale materials?* The present work addresses these questions using advanced experimental and theoretical techniques.

In particular, nanometer-sized metal particles supported on high surface area metal oxides display a rich variety of physicochemical properties that illustrate aspects of complexity due to environmental influences. It has been shown in both experiment and theory that the catalytic activity, selectivity, and stability of many types of supported metal catalysts depend not only on their structure, morphology, crystalline order, and charge state but also on the structural and electronic impacts that arise due to the interactions occurring with the support.^{17,18} For example, Frenkel et al.¹⁹ have shown that nanometer-sized Pt particles supported on different materials (γ -Al₂O₃ or carbon) with different adsorbates (CO or H) exhibit strong compressive strain only for the γ -Al₂O₃ support and CO, thus demonstrating the effects of both particle–support and particle–adsorbate bonding interactions on the catalyst structure. For the case of a weakly interacting support (carbon), Small et al.²⁰ have shown that the electronic density of 5d states (DOS) is influenced predominantly by the coverage of adsorbates, while thermal effects on the DOS are negligible. Support effects were investigated extensively by Koningsberger et al., who demonstrated that the support ionicity affects the CO and H₂ chemisorption properties of Pt

Received: August 25, 2015

Revised: October 20, 2015

Published: October 20, 2015

nanoparticles.^{21–26} The main challenge to resolve the mechanisms of catalytic activity mediated by the complex interactions of catalytic components of this type is largely one related to characterization methods, specifically in their capabilities to track the evolution of the structures of catalysts as occurs in response to changes in external conditions (e.g., high temperature and/or pressure). This type of analysis is now possible in the framework of *operando* methods of characterization developed in the past decade.^{27–33}

Much of the available literature that focuses on fundamental effects of the type described above is often qualitative in nature—presenting phenomenological descriptions of the structure–property correlations evidenced in catalytic processes. It is most notable that correlations of this form can now be treated in depth via theoretical modeling. In this regard, recent first-principles calculations of structural, electronic, and thermal properties of nanocatalysts have shown excellent agreement with experimental results obtained by X-ray absorption spectroscopy (XAS) methods.^{34–42} For this reason, theoretical methods have increasingly become an integral part of XAS data analysis and modeling.^{34,38,40} For example, following the observation of an anomalous thermal behavior, e.g., negative thermal expansion in the metal–metal bonds of Pt nanoparticles supported on Al₂O₃,⁴³ Vila et al. have shown that this effect arises, in part, due to the strongly inhomogeneous distribution of charges present in the metal clusters: atoms at the interface with the support were more positive than the atoms in the upper layers, which subsequently mediated the dynamical changes seen experimentally.³⁴ Such forms of heterogeneity of atoms and charges are not directly detectable by experimental methods such as XAS, since they measure ensemble-average properties and different models of either homo- or heterogeneously distorted atomic configurations can be developed that fit the experimental data equally well.^{44,45} Despite the increasingly important role that first-principles simulations of metal nanocatalysts have played here, theory and experiment often are not used synergistically. Rather, either experiment validates theory or theory informs experiment. This lack of synergism is a deficiency the current work directly addresses within the context of a study of environmental impacts on structural dynamics within catalytic materials.

From a characterization standpoint, the main challenge to *in situ* investigations is the need to capture important attributes of nanometer-sized catalysts with the desired spatial, temporal, and energy resolutions. Over the past decade, for example, the ability to characterize the electronic states of catalysts and their interactions with adsorbates has dramatically improved due to the development of new X-ray emission spectroscopy (XES) and combined XAS-XES methods, among which high energy resolution fluorescence detection (HERFD),^{11,46–48} and resonant inelastic X-ray scattering (RIXS) are the most important.^{49,50} Recent examples from the literature show that these spectroscopies make it possible to identify the specific adsorption sites of adsorbates (and the electronic effects of this binding),^{11,50} as well as the structural morphologies of the metal clusters mediating these interactions.⁵¹ Notable HERFD/RIXS studies of this type have been performed of the oxidation of CO over Pt/ γ -Al₂O₃ catalysts and the water gas shift reaction.^{52–56}

In the present work, we report an investigation of a model supported heterogeneous catalytic material, Pt on SiO₂, carried out using a synergistic combination of *in situ* RIXS and HERFD, and extended X-ray absorption fine structure

(EXAFS) spectroscopies, diffuse reflectance infrared Fourier transform spectroscopy (DRIFTS), mass spectroscopy, and *ex situ* electron microscopy studies, combined with first-principles theoretical modeling of both the dynamic structure of the systems and their spectroscopic behaviors. We show that this multimethod approach enables quantitative characterizations to be made of previously poorly understood cooperative effects in the structural dynamics of supported metal cluster catalysts. The system studied here experimentally, nanometer-sized Pt clusters supported on SiO₂ as exposed to H₂ or CO atmospheres at temperatures ranging from 300 to 700 K, is a prototypical heterogeneous catalyst. To simulate its properties theoretically, we investigated models of increasing complexity, ranging from single Pt atoms and small Pt clusters (both bare and CO-coordinated) to realistic *ab initio* models of supported nanocluster catalysts. We show here that these combined methods reveal markedly heterogeneous distributions of electronic charge that respond strongly to the environment—herein manifested as consequences of adsorbate coverage. Among the most significant points established in this work are that the environmental dynamics of charge localization observed in this prototypical system are both fluxional and invertible—a picture in which the most fundamental structure–property correlations for this supported metal cluster catalyst are underpinned by the strongly perturbative and heterogeneous contributions of metal–metal, metal–support, and metal–adsorbate bonding.

2. EXPERIMENTAL METHODS

A. Synthesis of Pt Catalysts. The Pt catalysts were prepared by wet impregnation of a soluble Pt precursor onto the SiO₂ support, followed by subsequent reduction in H₂ at elevated temperature. The catalyst weight loading was 1%. The procedure yielded small clusters with narrow dispersion in size (see below). A detailed description of the synthesis is given in the [Supporting Information](#).

B. Sample Characterization by STEM. High-angle annular dark-field scanning transmission electron microscopy (HAADF-STEM) measurements were carried out using a JEOL 2010F EF-FEG STEM (JEOL, Ltd.) to determine the size distributions of the supported catalyst particles. Details about the experimental setup, STEM samples, and particle size analysis are given in the [Supporting Information](#).

C. XAS/RIXS/HERFD Measurements. The EXAFS measurements at the Pt L₃-edge were carried out at the X19A beamline at the National Synchrotron Light Source at the Brookhaven National Laboratory. Comprehensive information about the experimental setups and the data analysis are provided in the [Supporting Information](#).

The RIXS/HERFD experiments were performed at the SuperXAS beamline⁵⁷ at the Swiss Light Source at the Paul Scherrer Institute. The experimental setup is schematically shown in [Figure 1a](#). During the measurement of the RIXS maps, the excitation energy E_{ex} was scanned across the Pt L₃-edge ($E_{\text{abs}} = 11563.7$ eV) from 11550 to 11630 or 11650 eV and the emission spectra were measured across the Pt L _{α 1} transition ($3d_{5/2} \rightarrow 2p_{3/2}$ transition, $E_{\text{em}} = 9442$ eV) from 9420 to 9480 eV using an energy-dispersive X-ray emission spectrometer with a von Hamos geometry.^{58,59} We used a cylindrically bent Ge(660) analyzer crystal ($R = 250$ mm) and a Pilatus 100k single-photon-counting pixel array detector.⁶⁰ The sample, the analyzer crystal, and the detector were arranged according to the vertical Rowland geometry. The combined

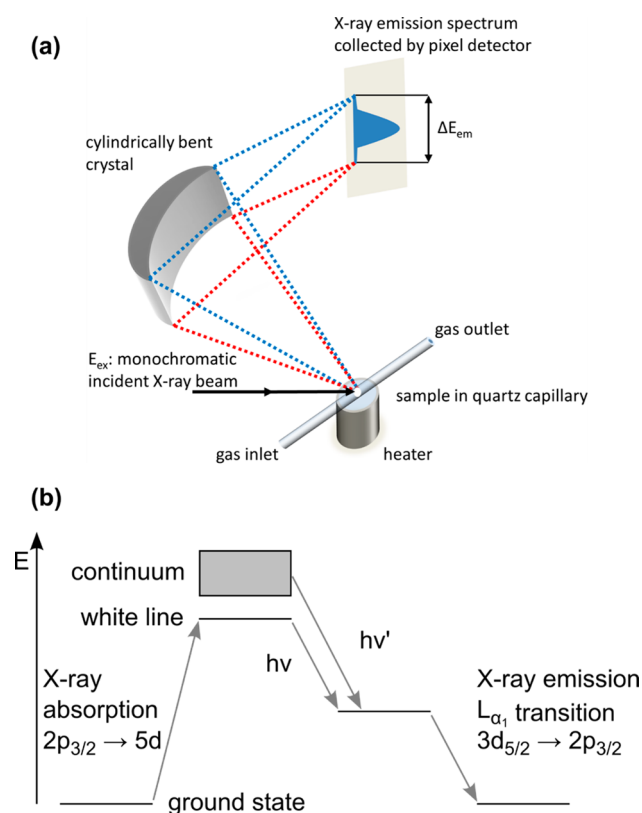


Figure 1. (a) Setup of the RIXS/HERFD experiment. (b) Electronic transitions probed in the RIXS/HERFD experiment.

incident energy resolution convoluted with the emitted energy resolution was about 1 eV at 80° (the Bragg angle of the analyzer crystal). HERFD spectra were extracted from the RIXS maps by averaging the excitation energies in the emission energy range from 9441.5 to 9442.5 eV. Further details about the experimental setup and data analysis are provided in the [Supporting Information](#).

D. DRIFTS Measurements. Diffuse reflectance infrared Fourier transform spectroscopy (DRIFTS) measurements were carried out using a Thermo-Nicolet 6700 IR spectrometer equipped with a Harrick DRIFTS cell. Additional experimental details are given in the [Supporting Information](#).

To obtain complementary XAS, RIXS/HERFD, and DRIFTS data of the supported catalyst, the samples were subjected to the same measurement procedure (varying gas atmosphere and temperature) at the different experimental setups. Each measurement was carried out under gas flow under steady-state conditions. In particular, the following procedure was applied: The pristine sample was exposed to He at 300 K. Then, it was reduced in H₂ at 700 K. Afterward, it was exposed to CO and the temperature was altered in multiple steps from 700 to 300 K and then returned to 700 K. Finally, the sample was reduced in H₂ at 700 and 300 K. A measurement was taken after each change. The last three measurements were performed to check the stability/reversibility.

3. THEORETICAL MODELING

A. Modeling of the Line Shifts. Among the most interesting behaviors of the *in situ* RIXS and HERFD experimental spectra are the changes in shape, intensity, and position of the characteristic lines and peaks of the X-ray emission and absorption spectra. To model the temperature-

induced changes in the absorption and emission energies observed under a CO atmosphere, we assume that they are caused largely by the changes in the electronic charges of the Pt atoms. For example, the charge distribution can change as a function of temperature due to changes in the adsorbate coverage (CO or H₂). As a simple starting model, we simulated the effect of varying coverage by changing the electronic charge in an isolated Pt atom. We evaluated the effect of the varying charge on the shifts in energies of both the absorption and the emission lines. In order to verify that the change in coverage and the change in charge are consistent (e.g., that CO withdraws the electron density from the cluster, not *vice versa*), we evaluated the effect of the CO ligands on Pt atoms using a model of a four-atom, unsupported, Pt cluster covered by CO molecules. Specifically, the DFT calculations were performed in two systems: (i) a Pt atom, and (ii) Pt₄ and Pt₄(CO)₄ clusters. The absorption energy was estimated from the difference between the occupied 2p_{3/2} and the first unoccupied states with large d character (>95%, compare with [Figure 1b](#)), while the emission energy was estimated as the difference between the energies of the occupied 3d_{5/2} and 2p_{3/2} states. For these calculations, the B3LYP exchange-correlation functional, with all-electron spin-orbit ZORA relativistic corrections and a [8s,7p,4d,2f] basis set for the Pt atom, was used. For the calculations involving the Pt atom, the effect of varying CO coverage was simulated by changing the total charge of the atom.

B. Modeling the Structural Changes in Clusters.

Quantitative data analysis of *in situ* EXAFS experiments, as shown below, was aided by first-principles simulations in order to enable more accurate insights into the structural motifs of the nanocatalysts and their dynamic changes with temperature. The structural effects observed in the experiments required a different set of models to aid the EXAFS data analysis that detects Pt–Pt interactions and interpret them in terms of the structure and dynamics of multiatom configurations. The simplest starting model has four Pt atoms covered by CO molecules, e.g., the same as the one used for modeling of the electronic effects. This model was used to test the effect of changing coverage on the Pt–Pt bond lengths. A more realistic model that included interactions with support and particle sizes compatible with those used in our experiments was constructed using a 37-atom Pt cluster. All optimizations and electron density calculations of the supported Pt₃₇ cluster were done with VASP using PAW pseudopotentials and a plane-wave cutoff of 400 eV.

The SiO₂ support was modeled using the (001) surface of α -quartz, i.e., the most stable dangling SiO₂ surface.^{61,62} This surface, however, is known to reconstruct,^{62–64} forming rings with six SiO units. The final surface for the simulations was, therefore, obtained by molecular dynamics (MD) annealing, followed by optimization (see the [Supporting Information](#) for details). The structure of the Pt₃₇ cluster was chosen to be consistent with the STEM and EXAFS results and corresponds to a hemi-cuboctahedron with a hexagonal base and composed of three atomic layers parallel to the support. This structure exposes both square (100) and triangular (111) facets. Single CO molecules or H atoms were adsorbed on representative edge and face top sites to study the local effects of adsorption. To study the effects of high coverage, either 15 CO molecules or 15 H atoms were adsorbed on the exposed on-top sites of the upper two layers of the cluster. The net charges were computed with the Bader density partition algorithm, using an

accurate VASP FFT grid to ensure precise electron counts up to 1×10^{-4} e.

4. RESULTS AND DISCUSSION

This section contains a summary of the major results obtained by combined experimental and theoretical methods. We start with a discussion of the experimental data analysis that incorporates the results of theoretical simulations and follow with a full treatment of the dynamics within the framework of theory.

A. Results of Imaging and Spectroscopy Experiments.

In this subsection, we summarize results of STEM, EXAFS, conventional and HERFD XANES, RIXS, and DRIFTS measurements. Taken together, these results suggest that variations of the electron charge in the cluster are the main driving force responsible for the changes observed in XAS and XES spectra. The origin of these charge changes is investigated theoretically in section 4B.

1. Nanoparticle Size before and after the XAS Experiments. Representative STEM images of the supported metal catalysts are provided in the Supporting Information (Figure S1). For the pristine Pt/SiO₂ catalyst, well-defined and narrow particle size distributions are obtained, as shown in the Supporting Information (Figure S2). The average particle size is 1.06 ± 0.27 nm (2273 particles). After the RIXS/HERFD experiments, the size distribution is very similar as before with an average particle size of 1.18 ± 0.33 nm (2930 particles), indicating that, within the limits of experimental uncertainty, the average particle size remains largely unaffected by the experimental procedures followed in the *in situ* measurements.

2. Geometrical and Electronic Structures Probed *In Situ*. For the Pt/SiO₂ catalyst, good EXAFS fits were obtained for all experimental conditions using fitting models including both first-shell Pt–Pt and Pt–low-Z-element (O/C) scattering paths, as described in the Supporting Information. In EXAFS analyses of temperature-resolved data, an analytical approach frequently used is to assume that the bond length disorder results from two contributions, which are either vibrational or configurational in nature. The former component depends on temperature, while the latter does not. This model, however, is not consistent with our main theoretical finding, as described in greater detail below, which shows that the configurational disorder present in this nanoscale material system varies significantly with temperature. For this reason, a different model was used in which the total disorder was varied independently at different temperatures.

The k^2 -weighted EXAFS oscillations $\chi(k)$ and the Fourier-transformed magnitudes $|\chi(r)|$ together with the best fits are given in the Supporting Information (Figure S3). The fitting results are shown in Figure 2 and the Supporting Information (Table S1, Figure S4).

The Pt–Pt coordination number was found to be 6.50 ± 0.31 , constant throughout all regimes of the experiment. Assuming simple face-centered cubic, truncated hemispherical cuboctahedral geometries for the supported Pt clusters, and given the narrow size distribution ascertained by STEM (Figure S2), this coordination number points to a “representative” cluster of 37 atoms and 1.1 nm in diameter.⁴⁴ The Pt–Pt bond distances are clearly shorter than the bulk Pt value of 2.77 Å. Specifically, they range between 2.72 and 2.74 Å in a H₂ atmosphere and between 2.75 and 2.76 Å in a CO atmosphere and decrease with temperature. These structural changes are explained by adsorbate-induced charge transfer altering the

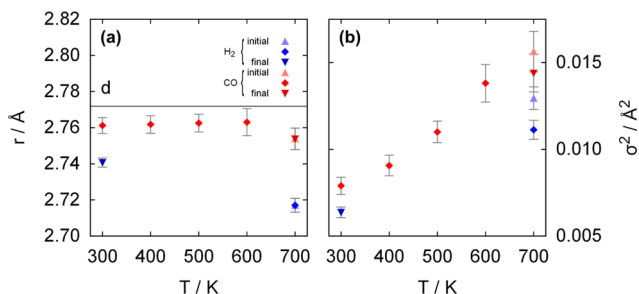


Figure 2. Temperature dependence of the (a) Pt–Pt bond length and (b) bond length disorders for Pt/SiO₂ in H₂ and CO.

character of the Pt–Pt bonds^{65,66} and are addressed in detail in the Theory section (*vide infra*). The coordination number of the Pt atoms with neighbors of low atomic number (it is not possible to distinguish between C or O, due to the similarity in their backscattering properties) denoted as “low Z”, is 0.97 ± 0.11 . The Pt–low-Z bond distances, ranging between 2.46 and 2.58 Å, are smaller by 0.1 Å in a H₂ than in CO atmospheres at the same temperatures. These contributions are likely to reflect the bonding with both the support and CO (when present). It is not possible, within the present models, to identify these contributions with higher certainty within the fitting done in the EXAFS analysis. Only by using a combination of EXAFS with other complementary experiments that have greater sensitivity to metal–adsorbate interaction (HERFD and DRIFTS), as well as DFT modeling, were we able to isolate the coverage effects on the electronic and structural effects exhibited by Pt atoms (*vide infra*).

Figure 2b shows the dependence of Pt–Pt bond length disorder on temperature. First-principles modeling results shown below present a picture of the simulated cluster that has very different structures at low and high temperature. In such case, the variation of the bond length disorder parameter with temperature should not be constrained by a commonly used correlated Einstein (or Debye) model⁶⁷ in which the total bond length disorder is a sum of two terms, the configurational (static) disorder and the vibrational disorder. According to these models, the latter term and hence the total disorder should vary linearly with temperature within the experimental temperature range, which is not a physically reasonable model for the case discussed here. Indeed, in our case, configurational and charge transformations that are predicted theoretically to occur during the temperature range studied are not consistent with constant static disorder. In that regard, our approach to the treatment of the bond length disorder is similar of those observed previously in systems with electronic and structural transitions.^{68,69}

The Pt–Pt bond distance disorder ranges from 60×10^{-4} to 160×10^{-4} Å², increasing with increasing temperature, as expected. In a H₂ atmosphere, the disorders are slightly lower (by $20\text{--}30 \times 10^{-4}$ Å²) than in a CO atmosphere at identical temperatures, indicative of reduced bond strains.¹⁹ The r -factor was found to be 0.007, indicative of the overall very good fitting quality.

3. Adsorption-Dependent Changes of the Electronic Landscape. Typical RIXS maps of the Pt/SiO₂ catalyst in H₂ and CO atmospheres at the external temperatures of 700 and 300 K are shown in Figure 3. In absorption, the Pt L₃-edge transition (i.e., the excitation of electrons from 2p_{3/2} to mainly 5d_{5/2} states) and, in emission, the L_{α1} transition (i.e., from 3d_{5/2}

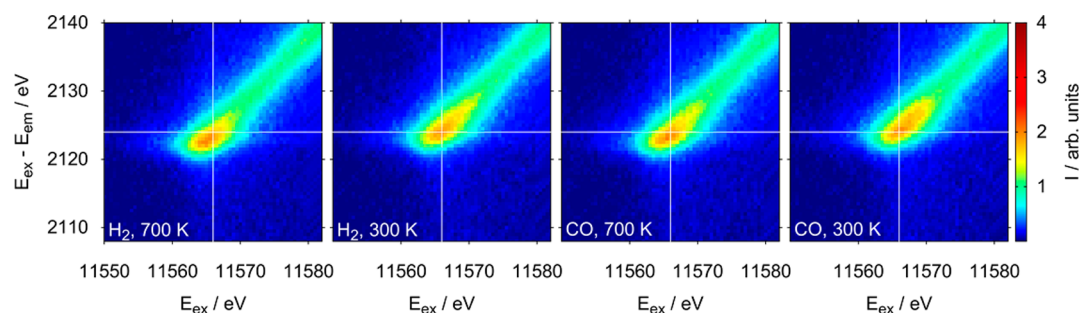


Figure 3. RIXS maps for Pt/SiO₂ in H₂ and CO at the extreme temperatures of 700 and 300 K. The horizontal axis shows the excitation energy and the vertical axis the difference between the excitation and emission energies.

to 2p_{3/2} states) are probed (Figure 1b).⁷⁰ In the H₂ and CO atmospheres, the RIXS maps reveal similar temperature dependencies. With decreasing temperature, the resonant peak shifts to higher excitation and emission energies, decreases in intensity, and changes its shape from a more circular to more elongated form. The variations seen are more pronounced for CO than for H₂. These findings are discussed together with the HERFD results below.

A comparison of the HERFD and conventional XANES spectra of the catalyst in H₂ and CO atmospheres at the extremal temperatures of 700 and 300 K is provided in Figure 4a,b. Because of the higher energy resolution of the partial

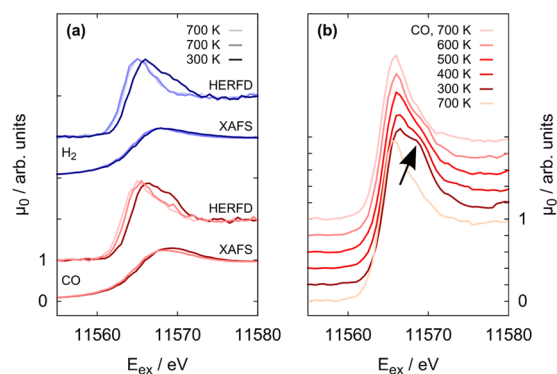


Figure 4. HERFD XANES and conventional XANES spectra for Pt/SiO₂ in (a) H₂ and CO at 700 and 300 K. (b) HERFD XANES spectra for Pt/SiO₂ in CO at various temperatures. The experimental sequence is shown from top to bottom. The arrow indicates the shoulder in the white line.

fluorescence yield detection in the order of the lifetime broadening of the final state,^{46,71} the HERFD XANES spectra exhibit superior characteristics (e.g., a sharper absorption edge, a sharper and more intense white line, as well as an additionally distinguishable feature in the white line) compared to the conventional XANES spectra (Figure 4a,b). In a H₂ atmosphere, the conventional XANES spectra do not vary strongly with temperature, except for a small shift of the absorption edge and white line.^{15,65,72} In contrast, the HERFD XANES spectra reveal a much stronger, reversible shift of both lines to higher energies with decreasing temperature. In addition, the white line is asymmetrically broadened at 300 K, i.e., exhibits a shoulder at ≈ 5 eV above the absorption peak maximum. In a CO atmosphere, similar trends are identified. In particular, the shoulder is more pronounced and thus its changes, albeit only very small, can already be distinguished in the conventional XANES spectra. The much more pronounced

changes in the HERFD XANES spectra (Figure S5) allow the quantitative analysis of the evolution of both the white line and its shoulder with temperature.

The RIXS maps in H₂ and CO atmospheres reveal very similar temperature-dependent shifts of the resonant lines. In two previous RIXS studies at the Pt L₃-edge (i.e., probing the 2p_{3/2}–5d_{5/2} transition both in absorption and in emission),^{20,50} analogous shifts of the resonant peak were reported. In one of these studies,²⁰ 1.25 nm Pt/C particles in H₂ and CO atmospheres at 307 and 673 K were investigated. The shifts were ≤ 0.4 eV and slightly larger in CO than in a H₂ atmosphere. Theoretical modeling taking temperature-induced disorder and coverage variations into account attributed the shifts to the latter.²⁰ In the other study,⁵⁰ the adsorption of CO on 1 nm Pt/ γ -Al₂O₃ at room temperature was explored and similar shifts and shape changes of the resonant peak as those identified in this work were found. Theoretical modeling not only assigned the shifts to CO adsorption, but also related them to a specific adsorption site of the CO molecules on the Pt atoms, namely, atop. That capability of XANES is thus complementary to DRIFTS. The similar RIXS/HERFD trends reported here and in those earlier studies suggest that the changes in the adsorbate coverage are responsible for our data as well.

For a quantitative assessment of their temperature dependencies, the HERFD absorption edge and white line energies were determined as the zero-crossings in the second- and first-derivative spectra, respectively, obtained via fitting of the two data points above and below each crossing (i.e., within ± 1 eV) with a line. As an example, the temperature dependence of the white line energy is shown in Figure 5a. The variations of the energies of both lines are very similar in H₂ and CO atmospheres; i.e., from 700 to 300 K, the shift to lower energies is seemingly linear and its maximum variation is 1.5 eV. Similar shifts of the absorption edge energy upon H and CO adsorption were previously reported for 1.4 nm Pt/ γ -Al₂O₃ and 1.7 nm Pt/SiO₂.⁷³ In bulk insulating compounds, e.g., oxides, absorption shifts are attributed to variations in the charge state of the X-ray absorbing atom and are thus routinely used for measuring the oxidation state of an element. These shifts stem from the decrease in screening of the positively charged nucleus by electrons of the same element in different oxidation states causing an increase of the ionization potential and, hence, of the absorption edge energy for elements with a larger formal oxidation state. In nanoparticles, however, charge transfer from metal atom to adsorbate (or support) not only does decrease the screening, thus tending to shift the absorption edge to higher energies, but also lowers the Fermi level, causing a tendency to shift the edge energy lower.¹⁹ It is,

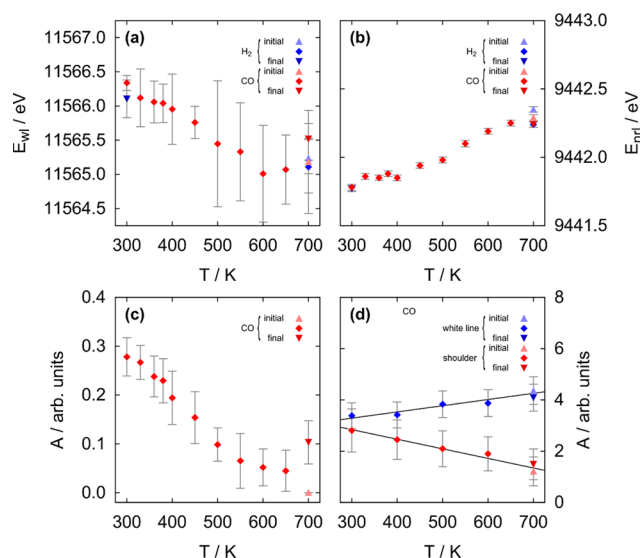


Figure 5. Temperature dependence of the (a) white line energy, (b) nonresonant line energy, (c) total differential white line area with respect to the initial spectrum in H₂ at 700 K, and (d) areas of the white line and shoulder for Pt/SiO₂ in CO as obtained in the fitting.

therefore, risky to rely only on the edge shift to determine the direction of the charge transfer, and other input is needed. A more detailed discussion is given in the Theory section.

The behaviors seen in the nonresonant regions of the RIXS data show an opposite trend compared to those observed in the resonant region. For a quantitative assessment of the temperature-dependent shifts of the nonresonant lines, the RIXS maps were combined in the incident energy range of 11590–11630 eV to yield averaged emission spectra. These spectra were fitted in the range of 9400–9480 eV of the emission energy values by a combination of a line and a Lorentzian with constrained amplitude and half-width for all data sets. The resulting data are shown in Figure 5b. The nonresonant line shifts linearly to lower energies with decreasing temperature, very similar in H₂ and CO atmospheres. In particular, from 700 to 300 K, the shift is -0.6 eV, in the opposite direction to the absorption edge line shift (*vide supra*). Such a shift has not, to the best of our knowledge, been reported before. As discussed in the Theory section below, it likely originates from the change in the charge state of the particles.

For the Pt L₃-edge, the white line area is proportional to the density of unoccupied d-states.^{74,75} This property can be used to quantitatively assess changes in the electronic structure of the catalysts¹⁵ due to the interactions variously occurring between the metal clusters, support, and adsorbates. The temperature dependence of the total differential white line area with respect to the initial spectrum measured at 700 K, integrated between 11558 and 11576 eV, in CO is shown in Figure 5c. A shoulder in the white line already has been reported before for Pt/ γ -Al₂O₃ in a CO atmosphere at room temperature.^{11,55} Theoretical modeling allows us to conclude that this shoulder is due to CO molecules adsorbed at top sites.¹¹ CO molecules adsorbed at other sites merely caused broadening of the white line.¹¹ This interpretation seems to be in agreement with the RIXS/HERFD results reported here.

To quantify the contributions of the white line and shoulder, the HERFD XANES spectra were fitted by a combination of a broadened error function (to account for the absorption edge)

and two Gaussians. The widths of the step function and each of the two Gaussians were constrained for all temperatures. The fitted areas of the white line and shoulder are shown in Figure 5d. Both peaks show linear, but opposite, temperature dependencies. While the area of the white line decreases, that of the shoulder increases with decreasing temperature. These changes yield direct insight into the coverages of two CO species adsorbed at different surface sites on the particles (cf. with the results of the DRIFTS measurements described below).

The changes in the conventional XAS white line area were used to assess the average transferred charge per Pt atom in the particles quantitatively. The Pt L₃ white line area is proportional to the density of unoccupied Pt 5d states and hence is commonly used for this type of analysis.^{75–78} Therefore, comparing the normalized relative white line areas $(A_1 - A_0)/A_0$, where A_0 represents the fully reduced sample at 700 K and A_1 the CO-covered sample at 300 K (~ 0.17), with that reported in the earlier publication (~ 0.80 per transferred electron) allows us to estimate that 0.21 electrons (the relative error is estimated as 20%) per Pt atom are transferred upon CO adsorption. This is in good agreement with the theoretical results (see below).

4. Analysis of the CO Coverage by DRIFTS. The adsorption of CO,^{79–88} the oxidation of CO,^{89,90} as well as the water–gas shift reaction^{91,92} over various kinds of Pt catalysts on multiple support materials (Pt/SiO₂, Pt/Al₂O₃) over broad pressure and temperature ranges have been studied comprehensively by infrared spectroscopy methods. In particular, various adsorption sites (linear, bridge, 3-fold) in clusters of different oxidation states^{81–88,93,94} and their temperature-dependent evolution have been identified.^{81–83,85,87} The apparently pronounced effects of the weight loading, particle morphology, and the support material on the spectroscopy have not been fully characterized to date.^{86,87} It is known, however, that the relative coverages of the different CO species (e.g., linear and bridge) vary sensitively with the acidity of the support.²² The CO saturation coverage on a specific type of supported Pt/SiO₂ catalyst at room temperature has been identified to be 0.6–0.7,⁸¹ i.e., is considerably lower than that for ideal Pt(111) surfaces.

Differential DRIFT spectra of Pt/SiO₂ in a CO atmosphere at temperatures between 700 and 300 K with respect to the initial spectrum of the clean, fully reduced sample in a H₂ atmosphere at 700 K are shown in Figure 6a. Pronounced spectral lines occur at 1890, 2060, 2110, and 2180 cm⁻¹, with decreasing intensities for each seen with increasing temperature. An additional mode at 1630 cm⁻¹ is present only at 300 K.

Fitting of the spectra was performed in the range between 1775 and 2250 cm⁻¹ using a combination of a local linear background and six Gaussians. In particular, for the most intense line at 2060 cm⁻¹, a combination of three Gaussians was required to account for its asymmetry. It was not possible to obtain adequate fits of the spectra measured at 700 K because of the low intensities. The widths of the Gaussians were each constrained for all temperatures. The dependencies of the fitted areas of the spectral lines on the temperature are shown in Figure 6b. The complete fitting results are given in the Supporting Information (Figure S6).

The spectral lines between 1890 and 2180 cm⁻¹ can be attributed to various forms of CO. The line at 1890 cm⁻¹ is due to a bridge-bond form of CO adsorbed on Pt.^{81–84,88,95} The

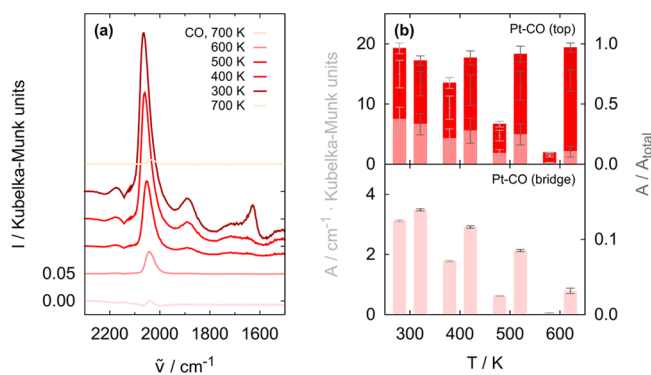


Figure 6. (a) Difference DRIFT spectra of Pt/SiO₂ in CO at various temperatures with respect to the initial spectrum in H₂ at 700 K. The spectra were stacked after subtraction of a background offset (determined as average intensity at around 2250 cm⁻¹). The experimental sequence is shown from bottom to top. (b) Temperature dependence of the absolute (left bars, brighter y-axis label) and relative areas (right bars, darker label) of the spectral lines due to CO adsorbed on top (three components; the darkest color corresponds to that at higher and the brightest at lower wavenumbers) and on bridge sites (one component), shown in the top and in the bottom of (b), respectively, obtained from the fitting. The complete fitting results are shown in the Supporting Information (Figure S6).

three lines between 2020 and 2060 cm⁻¹ are due to the top-bond form,^{81–84,88,94,95} for which the literature suggests different local bonding environments for the Pt atom contact lead to shifts in the mode frequency (individual bands in this latter range could not be distinguished due to the comparably low spectral resolution employed).^{88,94,95} The lines at 2110 and 2180 cm⁻¹ are the envelopes of the vibrational–rotational bands of gas-phase CO.^{96,97} The line at 1630 cm⁻¹, only present at 300 K, is likely due to the scissoring mode of water adsorbed on the silica support.⁹⁸

The frequency of the line due to bridge-bonded CO varies only weakly with temperature. In contrast, the frequencies for the top-bonded form(s) shift markedly (to higher frequencies) with decreasing temperature. Similar shifts have been identified previously, e.g., on Pt/Mg(Al)O,⁹⁵ and were related to the temperature dependence of the CO coverage as in the present case. The areas of all spectral lines increase approximately linearly with decreasing temperature (Figure 6b, left bars). It is evident that, even at the maximum temperature of 700 K, a small fractional coverage of CO is present in dynamic equilibrium on the Pt particles in this isobaric measurement and, in addition, that the fraction of the top-bonded form of CO present on the Pt clusters increases (and that of bridge-bonded form decreases) with decreasing temperature (Figure 6b, right bars). The latter are trends directly attributable to the temperature-dependent adsorbate coverage.

The changes seen in the ratio of top- and bridge-bond CO are in qualitative agreement with that obtained from fitting of the HERFD XANES spectra, i.e., the ratio of the areas of the white line and its shoulder. This is seemingly in contradiction with the results of an earlier theoretical XAS study of the CO adsorption sites on Pt₆ clusters, in which the shoulder in the white line was attributed to CO adsorbed on top, rather than bridge or 3-fold, sites.¹¹ The latter two species, however, also exhibit features in the energy range of the white line shoulder. The changes in relative coverage of these species are much less important than the changes in total coverage that is dominated by top-bonded species and decreases monotonically with

temperature. As such, the temperature dependences of the XANES white line and shoulder intensities seen here do, in fact, follow the interpretations given in the earlier literature, once the variations in the total as well as relative coverages of the different CO species (as revealed in the DRIFTS experiments) are taken into account.

B. Results of the First-Principles Simulations. In this subsection, the results of the theoretical simulations are summarized. As noted above, the experimental results are consistent with pronounced changes in the average charge present on the Pt atoms in response to changes made in temperature at constant adsorbate background pressure. Adsorbate coverage, of course, must vary over the range of temperatures investigated. Theory must account for and quantitatively treat the impacts of this effect on the spectroscopy. The model explored quantitatively in this section assumes that each CO molecule shifts electron density from the cluster, causing the change in the total cluster charge that is, therefore, related to the adsorbate coverage. An unanticipated effect was found in this modeling, namely, a new behavior that emerges when the size of simulated clusters increased from one/four atoms to those more closely matching experimental observations (tens of atoms). Here, we found that the intracuster charges in the metal particles vary dramatically, ranging from net positive to negative, depending on the location within the cluster, and with distributions that even invert when adsorbate coverage shifts as a consequence of temperature changes between the low and high coverage limits.

1. Geometric and Electronic Structure Changes upon CO Adsorption. *a. Unsupported Pt₄ Clusters.* To investigate the origin of changes in the Pt–Pt bond distances upon CO adsorption, simple models of a four-atom Pt cluster, bare and CO-covered, were tested first. The structures of unsupported Pt₄ and Pt₄(CO)₄ clusters were optimized, as described in the Theoretical Modeling section (see also Figure 7). The details of

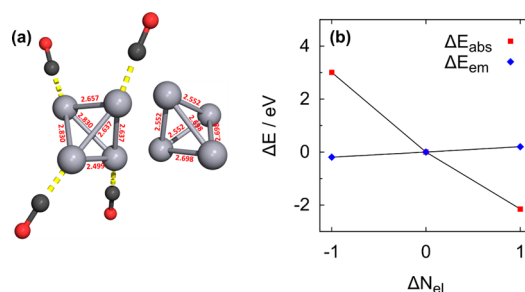


Figure 7. (a) Optimized cluster morphology of the Pt₄(CO)₄ and Pt₄ clusters. The reported distances are in Ångströms. (b) Shifts of the absorption edge and nonresonant emission energy calculated for an isolated Pt atom.

the Pt–Pt bond length distribution varied with the distance and orientation of the adsorbed CO molecules as expected for such a simple model (see Figure 7a); however, the Pt–Pt bond distances were found to increase upon adsorption. For all singlet and triplet multiplicity ground states, the average bond distance increased from 2.62 Å for the Pt₄ cluster to 2.70 Å for the Pt₄(CO)₄ cluster (by ≈3%). This change is larger than that obtained from the EXAFS fitting (0.7–1.7% comparing the H- and CO-covered particles at 300 and 700 K, respectively). This overestimation is probably due to (i) the fact that the experiments probed significantly larger particles, exhibiting smaller fractions of surface atoms, and (ii) the temperature-

dependent changes in CO coverage in the experiment were less than one over the range of temperatures studied, since DRIFTS results (Figure 6) demonstrated that, at the minimum temperature of 300 K, the particles were not fully CO-covered,⁸¹ while, at the maximum temperature of 700 K, they were not adsorbate-free.

b. Pt₃₇ Clusters on SiO₂ Support. In order to improve the theoretical estimates of bond expansion, simulations were performed for Pt₃₇ clusters on the SiO₂ support, since these systems were identified to be in best agreement with the average EXAFS coordination number and STEM particle sizes (*vide supra*). The structures of bare and various CO-covered clusters (i.e., with a CO molecule adsorbed at an edge or a face top site, or 15 CO molecules at the top sites of the surface atoms of the top and medium layers of the cluster to mimic high coverage, respectively) were optimized as described in the Theoretical Modeling section and are shown in Figure 8.

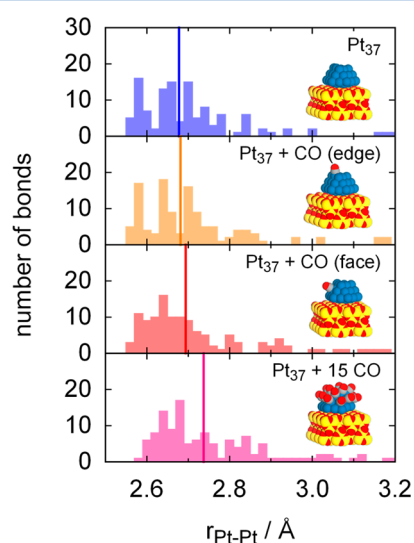


Figure 8. Changes of the Pt–Pt bond length upon CO adsorption for a simulated Pt₃₇ cluster on a SiO₂ support. The solid line corresponds to the centroid of the distribution. The bin size was 0.02 Å.

Clusters with CO molecules at bridge sites were neglected due to their relatively low coverages (*vide supra*). We have also avoided placing CO molecules at the sites interfacial with the support due to the computational limitations of such a model which requires a much larger area of the support surface than the one used in the current simulations scheme.

The effects of adsorption of a CO molecule on the local Pt–Pt bonding are summarized in Table 1. For edge-site adsorption, the average Pt–Pt bond distance increases by 0.07 Å, with a homogeneous expansion over all bonds. In contrast, for face-site adsorption, the expansions are larger for the longer bonds between the surface and internal Pt atoms. The reason for this enhanced expansion is clear when analyzing the local charge distributions (*vide infra*): While, in the clean cluster, the face atoms are nearly neutral when a molecule is adsorbed, they become markedly positive. This increases their Coulomb repulsion from the very positive atoms in the center of the cluster, resulting in an enhanced bond distance, similar to the mechanism described above in the alumina-supported cluster where the charge transfer is between the cluster and the oxygen vacancy in the support.³³ Thus, the increase in average bond distance is significantly larger, by 0.23 Å.

Table 1. DFT-Calculated Nearest-Neighbor Bond Lengths and Their Changes upon Adsorption of a CO Molecule on a Pt₃₇ Cluster Supported on SiO₂

bonds	Pt ₃₇ /SiO ₂					
	edge			face		
	$r_{\text{Pt}_{37}}/\text{Å}$	$r_{\text{Pt}_{37}\text{-CO}}/\text{Å}$	$\Delta r/\text{Å}$	$r_{\text{Pt}_{37}}/\text{Å}$	$r_{\text{Pt}_{37}\text{-CO}}/\text{Å}$	$\Delta r/\text{Å}$
1	2.56	2.62	0.06	2.55	2.61	0.06
2	2.64	2.70	0.06	2.58	2.67	0.09
3	2.64	2.70	0.06	2.60	2.67	0.07
4	2.73	2.81	0.08	2.60	2.67	0.07
5	2.73	2.81	0.08	2.77	3.30	0.53
5				2.77	3.30	0.53

Since EXAFS yields ensemble-averaged Pt–Pt bond distances, the average first-shell bond distance (see Figure 2a) is a good measure of structural changes. For determination of this quantity, the bond distances up to a cutoff of 3.1 Å were considered (i.e., corresponding to the region, where the pair distribution function exhibits a gap between the first and second coordination shell for bulk Pt). The average expansion upon adsorption of 15 CO molecules on the Pt₃₇ cluster is 0.05 Å (1.7%), in good agreement with the expansion of 0.7–1.7% obtained from the EXAFS analysis. Even a single CO molecule adsorbed on the simulated clusters (Figure 8) demonstrates the increased average Pt–Pt distance, illuminating both the roles of adsorbates, and their temperature-dependent coverage, in influencing the structural rearrangements of the metal catalysts.

The net charge distributions for the bare and the CO-covered Pt₃₇ clusters are shown in Figure 9a–d, while the charge for each Pt atom as a function of its distance to the support surface (defined as the average z-position of the atoms in the topmost layer) is shown in Figure S7 in the Supporting Information. For Pt atoms not coordinated by CO molecules, the nanoparticle layers have an alternating charging pattern, with the atoms in the bottom layer closest to the support surface positively charged, the slightly higher ones negative, those in the middle layer positive, and in the topmost layer mostly negative. The charge transfer between the Pt and O atoms is much smaller than that in Pt clusters on γ -Al₂O₃, for which a net transfer of 0.1–0.2 electrons has been identified,³⁴ showing that interactions between the metal clusters and the support are, in essence, negligible here. Upon adsorption of a CO molecule, the CO-coordinated Pt atoms lose 0.2–0.3 electrons on average, with those in the middle, positive layer losing more charge than those in the topmost, negative layer. Perhaps the most remarkable observation is that the charging effects induced by adsorption are quite local, with little or no redistribution of the charge. The only visible nonlocal effect is the charge inversion in the internal atoms for the high coverage system.

2. Temperature-Induced Shifts of the Absorption Edge and Core Emission Modeling of the Shifts Using Isolated Pt Atoms. As discussed above, one of the key experimental observations of this study is the opposite shifts in the absorption edge and core emission energies depending on the temperature. Our calculations on an isolated Pt atom reproduce these trends, showing that the absorption edge and core emission line both shift in opposite directions as a function of the change in number of electrons in the system, as shown in Figure 7b.

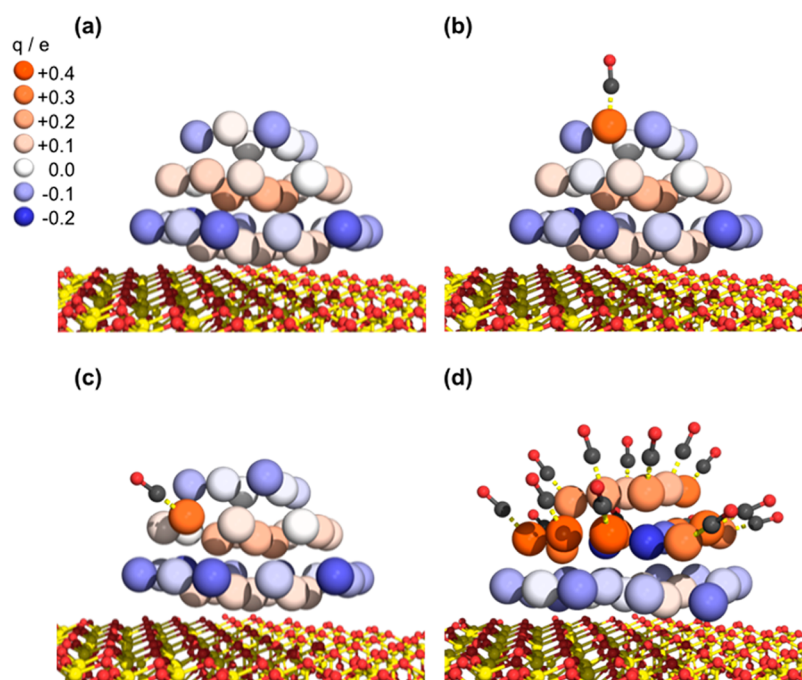


Figure 9. Charge transfer upon CO adsorption on a Pt₃₇ cluster on a SiO₂ support. Shown are the (a) bare cluster, one CO molecule adsorbed at top sites in an (b) edge and (c) face position, and (d) 15 adsorbed CO molecules to mimic high coverage.

The absorption edge exhibits a red shift with increasing cluster electron number (i.e., when the clusters become less positive). The emission line shows a small, but clear, trend in the opposite direction, in agreement with experiment. The shifts were obtained by averaging over different electronic configurations to account for the “mean” nature of an atom embedded in a cluster. The agreement between this model behavior and our experiment hints that the driving force behind the two shifts is the change in the adsorbate coverage that is affected by temperature. In order to verify this hypothesis, we need to verify that the increased temperature, and, hence, reduced coverage, results in the increase of the electronic charge of the cluster, to explain why the experimentally observed shifts and those calculated by this simple model are in the same direction.

As demonstrated above, these clusters exhibit strong heterogeneity in charge density. Hence, to verify the required correlation between coverage effects and charge density, we cannot use a simple 4-atom cluster model. Instead, our supported Pt₃₇ cluster models are more adequate, revealing a more complex picture of a heterogeneous charge distribution (*vide supra*) that also shows an overall loss of charge under increased coverage, but only after ensemble averaging. Therefore, the fact that, on supported Pt₃₇, the adsorbed CO and H remove electrons from the cluster leads to depleted electron densities at higher coverages and thus the correct absorption edge and emission line shift trends. The theoretical average electron loss per coordinated atom in Pt₃₇ is, however, about 0.2–0.3 e, somewhat less than the one used in the atomic simulations, and the shifts computed for the emission line energy should be considered qualitative. Nevertheless, we find that both the structural changes and the electronic changes in this system under variation in temperature are linked to the change in the adsorbate coverage.

5. SUMMARY AND CONCLUSIONS

This work demonstrates and clarifies the nature of heterogeneity of the structural and charge distributions within supported metal nanoparticles of the form used as heterogeneous catalysts. Theoretical structure models of SiO₂-supported Pt clusters, bare and coordinated by CO, were constructed to explain the changes in electronic properties as observed by XANES and RIXS. In simulating the CO coverage, only CO adsorbed at top sites was modeled by DFT, given that the fraction of bridge to top CO bonds was found to be small by *in situ* DRIFTS. Those models revealed that the atomic and charge distributions in the clusters changed upon varying adsorbate coverages. The DFT calculations confirmed that the shift of the absorption edge is caused by charge transfer from Pt to CO.

In this work, theoretical simulations were used in synergy with experimental observations to support these conclusions. Thus, theoretical simulations played an integral part in this study, going beyond fitting models to provide essential (and predictive) interpretations of the experimental data, and especially their heterogeneous structure. In this work, *ab initio* calculations were used to help at the critical stage of the EXAFS data analysis and modeling, when the decision is made how to analyze the temperature-dependent data. It is very common that such data are analyzed using either the Einstein or the Debye model, which assume that the static disorder is temperature-independent. Because the simulations were used early on in this work to investigate the perturbations of the electronic states observed in the nonresonant and resonant RIXS spectra, we used these simulations' results to guide EXAFS data modeling. Specifically, the simulations, demonstrating that, at different temperatures, the configurational bond length disorder changed (Figure 8), enabled a different type of analysis, in which the total disorder values at different temperatures were not constrained in the fit. That approach produced more detailed information about the structure than a

more approximate Einstein model that would have missed the most important result of this work, the intracluster heterogeneity.

We believe that this charge heterogeneity may provide an important new vantage point for assessing the key driving forces responsible for electronic and structural perturbations seen more generally in supported metal cluster catalysts under *operando* conditions. These results show that monometallic clusters exhibit similar behaviors to those previously observed in core-shell bimetallic catalysts that restructure under conditions of variable gas pressure and temperature.⁹⁹ Atomic species not only on the surface but also throughout the cluster respond dynamically to changing environmental conditions, accompanied by strong and even invertible forms of electron localization. We believe that these findings provide new insights into the nature of supported nanocatalysts that may provide important clues into their behavior.

■ ASSOCIATED CONTENT

📄 Supporting Information

The Supporting Information is available free of charge on the ACS Publications website at DOI: 10.1021/acs.jpcc.5b08267.

Details on nanoparticle synthesis; STEM, XAS, RIXS, and DRIFTS setup and measurements; DFT calculations; STEM images and particle size distributions; EXAFS, HERFD, and DRIFTS data; details of EXAFS fits; and charge transfer calculations upon CO adsorption on model clusters (PDF)

■ AUTHOR INFORMATION

Corresponding Authors

*E-mail: jjr@uw.edu (J.J.R.).

*E-mail: r-nuzzo@illinois.edu (R.G.N.).

*E-mail: anatoly.frenkel@yu.edu (A.J.F.).

Author Contributions

[▽]These authors contributed equally to this work.

Notes

The authors declare no competing financial interest.

■ ACKNOWLEDGMENTS

The authors gratefully acknowledge funding of this work by the Division of Chemical Sciences, Geosciences, and Biosciences within the U.S. Department of Energy, Office of Basic Energy Sciences, Catalysis Science Program, Grant No. DE-FG02-03ER15476, as well as the facilities support provided at the National Synchrotron Light Source at Brookhaven National Laboratory (U.S. Department of Energy, Office of Basic Energy Sciences, Contract No. DE-SC0012704), the Synchrotron Catalysis Consortium (U.S. Department of Energy, Office of Basic Energy Sciences, Grant No. DE-SC0012335), and computational support from NERSC, a DOE Office of Science User Facility, under Contract No. DE-AC02-05CH11231. The Swiss Light Source is gratefully acknowledged for beamtime provision under number 20130076. L. Baeni and E. de Boni are gratefully acknowledged for technical help at the SuperXAS beamline, and Dr. J. Szlachetko for useful discussions.

■ REFERENCES

(1) Sneed, B. T.; Young, A. P.; Tsung, C.-K. Building up strain in colloidal metal nanoparticle catalysts. *Nanoscale* **2015**, *7*, 12248–12265.

(2) Strasser, P.; Koh, S.; Anniyev, T.; Greeley, J.; More, K.; Yu, C.; Liu, Z.; Kaya, S.; Nordlund, D.; Ogasawara, H.; et al. Lattice-strain control of the activity in dealloyed core-shell fuel cell catalysts. *Nat. Chem.* **2010**, *2*, 454–460.

(3) *Nanomaterials: Synthesis, Properties and Applications*; Edelstein, A. S., Cammarata, R. C., Eds.; Institute of Physics Publishing: Bristol, Philadelphia, 1998.

(4) Robinson, I. Nanoparticle structure by coherent X-ray diffraction. *J. Phys. Soc. Jpn.* **2013**, *82*, 021012.

(5) Wasserman, H. J.; Vermaak, J. S. On the determination of a lattice contraction in very small silver particles. *Surf. Sci.* **1970**, *22*, 164–172.

(6) Buffat, P.; Borel, J. P. Size effect on the melting temperature of gold particles. *Phys. Rev. A: At, Mol., Opt. Phys.* **1976**, *13*, 2287–2298.

(7) Robinson, I.; Harder, R. Coherent X-ray diffraction imaging of strain at the nanoscale. *Nat. Mater.* **2009**, *8*, 291–298.

(8) Huang, W. J.; Sun, R.; Tao, J.; Menard, L. D.; Nuzzo, R. G.; Zuo, J. M. Coordination-dependent surface atomic contraction in nanocrystals revealed by coherent diffraction. *Nat. Mater.* **2008**, *7*, 308–313.

(9) Vicente, B. C.; Nelson, R. C.; Singh, J.; Scott, S. L.; van Bokhoven, J. A. Electronic structures of supported Pt and PtSn nanoparticles in the presence of adsorbates and during CO oxidation. *Catal. Today* **2011**, *160*, 137–143.

(10) Alayon, E. M. C.; Singh, J.; Nachtegaal, M.; Harfouche, M.; Bokhoven, J. A. v. In situ XAS probes partially oxidized platinum generating high activity for CO oxidation. *J. Phys.: Conf. Ser.* **2009**, *190*, 012152.

(11) Safonova, O. V.; Tromp, M.; van Bokhoven, J. A.; de Groot, F. M. F.; Evans, J.; Glatzel, P. Identification of CO adsorption sites in supported Pt catalysts using high-energy-resolution fluorescence detection X-ray spectroscopy. *J. Phys. Chem. B* **2006**, *110*, 16162–16164.

(12) Alexeev, O. S.; Chin, S. Y.; Engelhard, M. H.; Ortiz-Soto, L.; Amiridis, M. D. Effects of reduction temperature and metal-support interactions on the catalytic activity of Pt/ γ -Al₂O₃ and Pt/TiO₂ for the oxidation of CO in the presence and absence of H₂. *J. Phys. Chem. B* **2005**, *109*, 23430–23443.

(13) Mojet, B. L.; Koningsberger, D. C. CO-induced decomposition of small Pt particles in K-LTL zeolite. *Catal. Lett.* **1996**, *39*, 191–196.

(14) Tanaka, H.; Kuriyama, M.; Ishida, Y.; Ito, S.-i.; Tomishige, K.; Kunimori, K. Preferential CO oxidation in hydrogen-rich stream over Pt catalysts modified with alkali metals: Part II. Catalyst characterization and role of alkali metals. *Appl. Catal., A* **2008**, *343*, 117–124.

(15) Small, M. W.; Sanchez, S. I.; Marinkovic, N. S.; Frenkel, A. I.; Nuzzo, R. G. Influence of adsorbates on the electronic structure, bond strain, and thermal properties of an alumina-supported Pt catalyst. *ACS Nano* **2012**, *6*, 5583–5595.

(16) Bordiga, S.; Groppo, E.; Agostini, G.; van Bokhoven, J. A.; Lamberti, C. Reactivity of surface species in heterogeneous catalysts probed by in situ X-ray absorption techniques. *Chem. Rev.* **2013**, *113*, 1736–1850.

(17) Cuenya, B. R. Synthesis and catalytic properties of metal nanoparticles: Size, shape, support, composition, and oxidation state effects. *Thin Solid Films* **2010**, *518*, 3127–3150.

(18) White, R. J.; Luque, R.; Budarin, V. L.; Clark, J. H.; Macquarrie, D. J. Supported metal nanoparticles on porous materials. Methods and applications. *Chem. Soc. Rev.* **2009**, *38*, 481–494.

(19) Frenkel, A. I.; Small, M. W.; Smith, J. G.; Nuzzo, R. G.; Kvashnina, K. O.; Tromp, M. An in situ study of bond strains in 1 nm Pt catalysts and their sensitivities to cluster-support and cluster-adsorbate interactions. *J. Phys. Chem. C* **2013**, *117*, 23286–23294.

(20) Small, M. W.; Kas, J. J.; Kvashnina, K. O.; Rehr, J. J.; Nuzzo, R. G.; Tromp, M.; Frenkel, A. I. Effects of adsorbate coverage and bond-length disorder on the d-band center of carbon-supported Pt catalysts. *ChemPhysChem* **2014**, *15*, 1569–1572.

(21) Stakheev, A. Y.; Zhang, Y.; Ivanov, A. V.; Baeva, G. N.; Ramaker, D. E.; Koningsberger, D. C. Separation of geometric and electronic effects of the support on the CO and H₂ chemisorption properties of

supported Pt particles: The effect of ionicity in modified alumina supports. *J. Phys. Chem. C* **2007**, *111*, 3938–3948.

(22) Mojet, B. L.; Miller, J. T.; Koningsberger, D. C. The effect of CO adsorption at room temperature on the structure of supported Pt particles. *J. Phys. Chem. B* **1999**, *103*, 2724–2734.

(23) Ramaker, D. E.; Teliska, M.; Zhang, Y.; Stakheev, A. Y.; Koningsberger, D. C. Understanding the influence of support alkalinity on the hydrogen and oxygen chemisorption properties of Pt particles Comparison of X-ray absorption near edge data from gas phase and electrochemical systems. *Phys. Chem. Chem. Phys.* **2003**, *5*, 4492–4501.

(24) Oudenhuijzen, M. K.; van Bokhoven, J. A.; Miller, J. T.; Ramaker, D. E.; Koningsberger, D. C. Three-site model for hydrogen adsorption on supported platinum particles: Influence of support ionicity and particle size on the hydrogen coverage. *J. Am. Chem. Soc.* **2005**, *127*, 1530–1540.

(25) Oudenhuijzen, M. K.; van Bokhoven, J. A.; Ramaker, D. E.; Koningsberger, D. C. Theoretical study on Pt particle adsorbate bonding: Influence of support ionicity and implications for catalysis. *J. Phys. Chem. B* **2004**, *108*, 20247–20254.

(26) Ji, Y.; Koot, V.; van der Eerden, A. M. J.; Weckhuysen, B. M.; Koningsberger, D. C.; Ramaker, D. E. A three-site Langmuir adsorption model to elucidate the temperature, pressure, and support dependence of the hydrogen coverage on supported Pt particles. *J. Catal.* **2007**, *245*, 415–427.

(27) Bañares, M. A.; Wachs, I. E. Molecular structures of supported metal oxide catalysts under different environments. *J. Raman Spectrosc.* **2002**, *33*, 359–380.

(28) Topsøe, H. Developments in operando studies and in situ characterization of heterogeneous catalysts. *J. Catal.* **2003**, *216*, 155–164.

(29) Weckhuysen, B. M. Determining the active site in a catalytic process: Operando spectroscopy is more than a buzzword. *Phys. Chem. Chem. Phys.* **2003**, *5*, 4351–4360.

(30) Molenbroek, A.; Helveg, S.; Topsøe, H.; Clausen, B. Nanoparticles in heterogeneous catalysis. *Top. Catal.* **2009**, *52*, 1303–1311.

(31) Bañares, M. A. Operando spectroscopy: The knowledge bridge to assessing structure–performance relationships in catalyst nanoparticles. *Adv. Mater.* **2011**, *23*, 5293–5301.

(32) Frenkel, A. I.; Rodriguez, J. A.; Chen, J. G. Synchrotron techniques for in situ catalytic studies: Capabilities, challenges, and opportunities. *ACS Catal.* **2012**, *2*, 2269–2280.

(33) Li, Y.; Zakharov, D.; Zhao, S.; Tappero, R.; Jung, U.; Elsen, A.; Baumann, P.; Nuzzo, R. G.; Stach, E. A.; Frenkel, A. I. Complex structural dynamics of nanocatalysts revealed in operando conditions by correlated imaging and spectroscopy probes. *Nat. Commun.* **2015**, *6*, 7583.

(34) Vila, F.; Rehr, J. J.; Kas, J.; Nuzzo, R. G.; Frenkel, A. I. Dynamic structure in supported Pt nanoclusters: Real-time density functional theory and x-ray spectroscopy simulations. *Phys. Rev. B: Condens. Matter Mater. Phys.* **2008**, *78*, 121404.

(35) Rehr, J. J.; Vila, F. D. Dynamic structural disorder in supported nanoscale catalysts. *J. Chem. Phys.* **2014**, *140*, 134701.

(36) Vila, F. D.; Rehr, J. J.; Kelly, S. D.; Bare, S. R. Operando effects on the structure and dynamics of Pt_nSn_m/γ-Al₂O₃ from Ab initio molecular dynamics and X-ray absorption spectra. *J. Phys. Chem. C* **2013**, *117*, 12446–12457.

(37) Chill, S. T.; Anderson, R. M.; Yancey, D. F.; Frenkel, A. I.; Crooks, R. M.; Henkelman, G. Probing the limits of conventional extended X-ray absorption fine structure analysis using thiolated gold nanoparticles. *ACS Nano* **2015**, *9*, 4036–4042.

(38) Yancey, D. F.; Chill, S. T.; Zhang, L.; Frenkel, A. I.; Henkelman, G.; Crooks, R. M. A theoretical and experimental examination of systematic ligand-induced disorder in Au dendrimer-encapsulated nanoparticles. *Chem. Sci.* **2013**, *4*, 2912–2921.

(39) Roscioni, O. M.; Zonias, N.; Price, S. W. T.; Russell, A. E.; Comaschi, T.; Skylaris, C.-K. Computational prediction of L₃ EXAFS spectra of gold nanoparticles from classical molecular dynamics simulations. *Phys. Rev. B: Condens. Matter Mater. Phys.* **2011**, *83*, 115409.

(40) Price, S. W. T.; Zonias, N.; Skylaris, C.-K.; Hyde, T. I.; Ravel, B.; Russell, A. E. Fitting EXAFS data using molecular dynamics outputs and a histogram approach. *Phys. Rev. B: Condens. Matter Mater. Phys.* **2012**, *85*, 075439.

(41) Behafarid, F.; Ono, L. K.; Mostafa, S.; Croy, J. R.; Shafai, G.; Hong, S.; Rahman, T. S.; Bare, S. R.; Roldan Cuenya, B. Electronic properties and charge transfer phenomena in Pt nanoparticles on γ-Al₂O₃: size, shape, support, and adsorbate effects. *Phys. Chem. Chem. Phys.* **2012**, *14*, 11766–11779.

(42) Roldan Cuenya, B.; Alcántara Ortigoza, M.; Ono, L. K.; Behafarid, F.; Mostafa, S.; Croy, J. R.; Paredis, K.; Shafai, G.; Rahman, T. S.; Li, L.; Zhang, Z.; Yang, J. C.; et al. Thermodynamic properties of Pt nanoparticles: Size, shape, support, and adsorbate effects. *Phys. Rev. B: Condens. Matter Mater. Phys.* **2011**, *84*, 245438.

(43) Kang, J. H.; Menard, L. D.; Nuzzo, R. G.; Frenkel, A. I. Unusual non-bulk properties in nanoscale materials: Thermal metal-metal bond contraction of gamma-alumina-supported Pt catalysts. *J. Am. Chem. Soc.* **2006**, *128*, 12068–12069.

(44) Erickson, E. M.; Oruc, M. E.; Wetzel, D. J.; Cason, M. W.; Hoang, T. T. H.; Small, M. W.; Li, D.; Frenkel, A. I.; Gewirth, A. A.; Nuzzo, R. G. A comparison of atomistic and continuum approaches to the study of bonding dynamics in electrocatalysis: Microcantilever stress and in situ EXAFS observations of platinum Bond expansion due to oxygen adsorption during the oxygen reduction reaction. *Anal. Chem.* **2014**, *86*, 8368–8375.

(45) Yevick, A.; Frenkel, A. I. Effects of surface disorder on EXAFS modeling of metallic clusters. *Phys. Rev. B: Condens. Matter Mater. Phys.* **2010**, *81*, 115451.

(46) Hämäläinen, K.; Siddons, D. P.; Hastings, J. B.; Berman, L. E. Elimination of the inner-shell lifetime broadening in X-ray-absorption spectroscopy. *Phys. Rev. Lett.* **1991**, *67*, 2850–2853.

(47) Pushkar, Y.; Yano, J.; Glatzel, P.; Messinger, J.; Lewis, A.; Sauer, K.; Bergmann, U.; Yachandra, V. Structure and orientation of the Mn₄Ca cluster in plant photosystem II membranes studied by polarized range-extended X-ray absorption spectroscopy. *J. Biol. Chem.* **2006**, *282*, 7198–7208.

(48) Yano, J.; Kern, J.; Pushkar, Y.; Sauer, K.; Glatzel, P.; Bergmann, U.; Messinger, J.; Zouni, A.; Yachandra, V. K. High-resolution structure of the photosynthetic Mn₄Ca catalyst from X-ray spectroscopy. *Philos. Trans. R. Soc., B* **2008**, *363*, 1139–1147.

(49) Glatzel, P.; Bergmann, U. High resolution 1s core hole X-ray spectroscopy in 3d transition metal complexes—electronic and structural information. *Coord. Chem. Rev.* **2005**, *249*, 65–95.

(50) Glatzel, P.; Singh, J.; Kvashnina, K. O.; van Bokhoven, J. A. In situ characterization of the 5d density of states of Pt nanoparticles upon adsorption of CO. *J. Am. Chem. Soc.* **2010**, *132*, 2555–2557.

(51) Gorczyca, A.; Moizan, V.; Chizallet, C.; Proux, O.; Del Net, W.; Lahera, E.; Hazemann, J.-L.; Raybaud, P.; Joly, Y. Monitoring morphology and hydrogen coverage of nanometric Pt/γ-Al₂O₃ particles by in situ HERFD–XANES and quantum simulations. *Angew. Chem.* **2014**, *126*, 12634–12637.

(52) Singh, J.; Alayon, E. M. C.; Tromp, M.; Safonova, O. V.; Glatzel, P.; Nachtegaal, M.; Frahm, R.; van Bokhoven, J. A. Generating highly active partially oxidized platinum during oxidation of carbon monoxide over Pt/Al₂O₃: In situ, time-resolved, and high-energy-resolution X-ray absorption spectroscopy. *Angew. Chem., Int. Ed.* **2008**, *47*, 9260–9264.

(53) Singh, J.; Tromp, M.; Safonova, O. V.; Glatzel, P.; van Bokhoven, J. A. In situ XAS with high-energy resolution: The changing structure of platinum during the oxidation of carbon monoxide. *Catal. Today* **2009**, *145*, 300–306.

(54) Singh, J.; Lamberti, C.; van Bokhoven, J. A. Advanced X-ray absorption and emission spectroscopy: In situ catalytic studies. *Chem. Soc. Rev.* **2010**, *39*, 4754–4766.

(55) Singh, J.; Nelson, R. C.; Vicente, B. C.; Scott, S. L.; van Bokhoven, J. A. Electronic structure of alumina-supported monometallic Pt and bimetallic PtSn catalysts under hydrogen and carbon monoxide environment. *Phys. Chem. Chem. Phys.* **2010**, *12*, 5668–5677.

- (56) Singh, J.; van Bokhoven, J. A. Structure of alumina supported platinum catalysts of different particle size during CO oxidation using in situ IR and HERFD XAS. *Catal. Today* **2010**, *155*, 199–205.
- (57) Abdala, P. M.; Safonova, O. V.; Wiker, G.; van Beek, W.; Emerich, H.; van Bokhoven, J. A.; Sa, J.; Szlachetko, J.; Nachtegaal, M. Scientific opportunities for heterogeneous catalysis research at the SuperXAS and SNBL beam lines. *Chimia* **2012**, *66*, 699–705.
- (58) Hámos, L. V. X-ray micro-analyser. *J. Sci. Instrum.* **1938**, *15*, 87.
- (59) Szlachetko, J.; Nachtegaal, M.; de Boni, E.; Willmann, M.; Safonova, O.; Sa, J.; Smolentsev, G.; Szlachetko, M.; van Bokhoven, J. A.; Dousse, J.-C.; et al. A von Hamos x-ray spectrometer based on a segmented-type diffraction crystal for single-shot X-ray emission spectroscopy and time-resolved resonant inelastic X-ray scattering studies. *Rev. Sci. Instrum.* **2012**, *83*, 103105.
- (60) Kraft, P.; Bergamaschi, A.; Broennimann, C.; Dinapoli, R.; Eikenberry, E. F.; Henrich, B.; Johnson, I.; Mozzanica, A.; Schlepütz, C. M.; Willmott, P. R.; et al. Performance of single-photon-counting PILATUS detector modules. *J. Synchrotron Radiat.* **2009**, *16*, 368–375.
- (61) Rignanese, G. M.; De Vita, A.; Charlier, J. C.; Gonze, X.; Car, R. First-principles molecular-dynamics study of the (0001) α -quartz surface. *Phys. Rev. B: Condens. Matter Mater. Phys.* **2000**, *61*, 13250–13255.
- (62) Goumans, T. P. M.; Wander, A.; Brown, W. A.; Catlow, C. R. A. Structure and stability of the (001) α -quartz surface. *Phys. Chem. Chem. Phys.* **2007**, *9*, 2146–2152.
- (63) Murashov, V. V. Reconstruction of pristine and hydrolyzed quartz surfaces. *J. Phys. Chem. B* **2005**, *109*, 4144–4151.
- (64) Chen, Y.-W.; Cao, C.; Cheng, H.-P. Finding stable α -quartz (0001) surface structures via simulations. *Appl. Phys. Lett.* **2008**, *93*, 181911.
- (65) Reifsnnyder, S. N.; Otten, M. M.; Sayers, D. E.; Lamb, H. H. Hydrogen chemisorption on silica-supported Pt clusters: In situ X-ray absorption spectroscopy. *J. Phys. Chem. B* **1997**, *101*, 4972–4977.
- (66) Koningsberger, D. C.; Oudenhuijzen, M. K.; Bitter, J. H.; Ramaker, D. E. Study of geometrical and electronic effects induced by hydrogen chemisorption on supported Pt particles. Analysis of Pt–H EXAFS and Pt–H anti-bonding state shape resonances. *Top. Catal.* **2000**, *10*, 167–177.
- (67) Frenkel, A. I.; Rehr, J. J. Thermal expansion and X-ray-absorption fine-structure cumulants. *Phys. Rev. B: Condens. Matter Mater. Phys.* **1993**, *48*, 585–588.
- (68) Booth, C. H.; Bridges, F.; Kwei, G. H.; Lawrence, J. M.; Cornelius, A. L.; Neumeier, J. J. Direct relationship between magnetism and MnO_6 distortions in $\text{La}_{1-x}\text{Ca}_x\text{MnO}_3$. *Phys. Rev. Lett.* **1998**, *80*, 853–856.
- (69) Booth, C. H.; Bridges, F.; Kwei, G. H.; Lawrence, J. M.; Cornelius, A. L.; Neumeier, J. J. Lattice effects in $\text{La}_{1-x}\text{Ca}_x\text{MnO}_3$ ($x = 0 \rightarrow 1$): Relationships between distortions, charge distribution, and magnetism. *Phys. Rev. B: Condens. Matter Mater. Phys.* **1998**, *57*, 10440–10454.
- (70) Glatzel, P.; Sikora, M.; Smolentsev, G.; Fernández-García, M. Hard X-ray photon-in photon-out spectroscopy. *Catal. Today* **2009**, *145*, 294–299.
- (71) de Groot, F. M. F.; Krisch, M. H.; Vogel, J. Spectral sharpening of the Pt L edges by high-resolution X-ray emission. *Phys. Rev. B: Condens. Matter Mater. Phys.* **2002**, *66*, 195112.
- (72) Bus, E.; van Bokhoven, J. A. Hydrogen chemisorption on supported platinum, gold, and platinum-gold-alloy catalysts. *Phys. Chem. Chem. Phys.* **2007**, *9*, 2894–2902.
- (73) Guo, N.; Fingland, B. R.; Williams, W. D.; Kispersky, V. F.; Jelic, J.; Delgass, W. N.; Ribeiro, F. H.; Meyer, R. J.; Miller, J. T. Determination of CO, H_2O and H_2 coverage by XANES and EXAFS on Pt and Au during water gas shift reaction. *Phys. Chem. Chem. Phys.* **2010**, *12*, 5678–5693.
- (74) Lytle, F. W. Determination of d-band occupancy in pure metals and supported catalysts by measurement of the LIII X-ray absorption threshold. *J. Catal.* **1976**, *43*, 376–379.
- (75) Lytle, F. W.; Wei, P. S. P.; Gregor, R. B.; Via, G. H.; Sinfelt, J. H. Effect of chemical environment on magnitude of X-ray absorption resonance at L_{III} edges. Studies on metallic elements, compounds, and catalysts. *J. Chem. Phys.* **1979**, *70*, 4849–4855.
- (76) Erickson, E. M.; Thorum, M. S.; Vasić, R.; Marinković, N. S.; Frenkel, A. I.; Gewirth, A. A.; Nuzzo, R. G. In situ electrochemical X-ray absorption spectroscopy of oxygen reduction electrocatalysis with high oxygen flux. *J. Am. Chem. Soc.* **2012**, *134*, 197–200.
- (77) Yoshida, H.; Nonoyama, S.; Yazawa, Y.; Hattori, T. Quantitative determination of platinum oxidation state by XANES analysis. *Phys. Scr.* **2005**, *2005*, 813.
- (78) Mansour, A. N.; Cook, J. W.; Sayers, D. E. Quantitative technique for the determination of the number of unoccupied d-electron states in a platinum catalyst using the $L_{2,3}$ X-ray absorption edge spectra. *J. Phys. Chem.* **1984**, *88*, 2330–2334.
- (79) Lamberti, C.; Zecchina, A.; Groppo, E.; Bordiga, S. Probing the surfaces of heterogeneous catalysts by in situ IR spectroscopy. *Chem. Soc. Rev.* **2010**, *39*, 4951–5001.
- (80) Anderson, J. A.; Chong, F. K.; Rochester, C. H. IR study of CO adsorption on Pt, Re and Pt–Re/ Al_2O_3 catalysts before and after coking. *J. Mol. Catal. A: Chem.* **1999**, *140*, 65–80.
- (81) Podkolzin, S. G.; Shen, J.; de Pablo, J. J.; Dumesic, J. A. Equilibrated adsorption of CO on silica-supported Pt catalysts. *J. Phys. Chem. B* **2000**, *104*, 4169–4180.
- (82) Dulaurent, O.; Bianchi, D. Adsorption isobars for CO on a Pt/ Al_2O_3 catalyst at high temperatures using FTIR spectroscopy: isosteric heat of adsorption and adsorption model. *Appl. Catal., A* **2000**, *196*, 271–280.
- (83) Bourane, A.; Dulaurent, O.; Bianchi, D. Heats of adsorption of linear and multibound adsorbed CO species on a Pt/ Al_2O_3 catalyst using in situ infrared spectroscopy under adsorption equilibrium. *J. Catal.* **2000**, *196*, 115–125.
- (84) Bourane, A.; Dulaurent, O.; Bianchi, D. Comparison of the coverage of the linear CO species on Pt/ Al_2O_3 measured under adsorption equilibrium conditions by using FTIR and mass spectroscopy. *J. Catal.* **2000**, *195*, 406–411.
- (85) Bourane, A.; Dulaurent, O.; Bianchi, D. Heats of adsorption of the linear CO species adsorbed on a Pt/ Al_2O_3 catalyst in the presence of coadsorbed species using FTIR spectroscopy. *Langmuir* **2001**, *17*, 5496–5502.
- (86) Bourane, A.; Bianchi, D. Heats of adsorption of the linear CO species on Pt/ Al_2O_3 using infrared spectroscopy: impact of the Pt dispersion. *J. Catal.* **2003**, *218*, 447–452.
- (87) Pillonel, P.; Derrouiche, S.; Bourane, A.; Gaillard, F.; Vernoux, P.; Bianchi, D. Impact of the support on the heat of adsorption of the linear CO species on Pt-containing catalysts. *Appl. Catal., A* **2005**, *278*, 223–231.
- (88) Raskó, J. CO-induced surface structural changes of Pt on oxide-supported Pt catalysts studied by DRIFTS. *J. Catal.* **2003**, *217*, 478–486.
- (89) Schubert, M. M.; Kahlich, M. J.; Gasteiger, H. A.; Behm, R. J. Correlation between CO surface coverage and selectivity/kinetics for the preferential CO oxidation over Pt/ $\gamma\text{-Al}_2\text{O}_3$ and Au/ $\alpha\text{-Fe}_2\text{O}_3$: an in situ DRIFTS study. *J. Power Sources* **1999**, *84*, 175–182.
- (90) Maillard, F.; Savinova, E. R.; Simonov, P. A.; Zaikovskii, V. I.; Stimming, U. Infrared spectroscopic study of CO adsorption and electro-oxidation on carbon-supported Pt nanoparticles: Interparticle versus intraparticle heterogeneity. *J. Phys. Chem. B* **2004**, *108*, 17893–17904.
- (91) Busca, G.; Finocchio, E.; Escibano, V. S. Infrared studies of CO oxidation by oxygen and by water over Pt/ Al_2O_3 and Pd/ Al_2O_3 catalysts. *Appl. Catal., B* **2012**, *113–114*, 172–179.
- (92) Robbins, J. L.; Marucchi-Soos, E. Evidence for multiple carbon monoxide hydrogenation pathways on platinum alumina. *J. Phys. Chem.* **1989**, *93*, 2885–2888.
- (93) Haaland, D. M. Infrared studies of CO adsorbed on Pt/ Al_2O_3 : Evidence for CO bonded in 3-fold coordination. *Surf. Sci.* **1987**, *185*, 1–14.
- (94) Kappers, M. J.; van der Maas, J. H. Correlation between CO frequency and Pt coordination number. A DRIFT study on supported Pt catalysts. *Catal. Lett.* **1991**, *10*, 365–373.

(95) Gandao, Z.; Coq, B.; de Ménorval, L. C.; Tichit, D. Comparative behaviour of extremely dispersed Pt/Mg(Al)O and Pt/Al₂O₃ for the chemisorption of hydrogen, CO and CO₂. *Appl. Catal., A* **1996**, *147*, 395–406.

(96) Gracia, F. J.; Bollmann, L.; Wolf, E. E.; Miller, J. T.; Kropf, A. J. In situ FTIR, EXAFS, and activity studies of the effect of crystallite size on silica-supported Pt oxidation catalysts. *J. Catal.* **2003**, *220*, 382–391.

(97) Carlsson, P.-A.; Österlund, L.; Thormählen, P.; Palmqvist, A.; Fridell, E.; Jansson, J.; Skoglundh, M. A transient in situ FTIR and XANES study of CO oxidation over Pt/Al₂O₃ catalysts. *J. Catal.* **2004**, *226*, 422–434.

(98) Socrates, G. *Infrared and Raman Characteristic Group Frequencies: Tables and Charts*; John Wiley & Sons: Chichester, U.K., 2004.

(99) Nashner, M. S.; Frenkel, A. I.; Somerville, D.; Hills, C. W.; Shapley, J. R.; Nuzzo, R. G. Core shell inversion during nucleation and growth of bimetallic Pt/Ru nanoparticles. *J. Am. Chem. Soc.* **1998**, *120*, 8093–8101.